Earth and Planetary Science Letters 299 (2010) 91–103

Contents lists available at ScienceDirect

Earth and Planetary Science Letters

journal homepage: www.elsevier.com/locate/epsl

Stratification of the Earth beneath the Azores from P and S receiver functions

G. Silveira [a,b,*], L. Vinnik [c], E. Stutzmann [d], V. Farra [d], S. Kiselev [c], I. Morais [a]

[a] Instituto Dom Luiz, Campo Grande, Edificio C8, 1749-016 Lisboa, Portugal
[b] Área Científica de Física, Instituto Superior de Engenharia de Lisboa, 1959-007 Lisboa, Portugal
[c] Institute of Physics of the Earth, B. Grouzinskaya 10, Moscow 123995, Russian Federation
[d] Institut de Physique du Globe de Paris - Paris Sorbonne Cite - CNRS UMR 7154, 1 rue Jussieu, 75005 Paris, France

ARTICLE INFO

Article history:
Received 19 February 2010
Received in revised form 6 August 2010
Accepted 13 August 2010
Available online 20 September 2010

Editor: L. Stixrude

Keywords:
receiver functions
hotspots
mantle transition zone
Azores

ABSTRACT

Seismic recordings of IRIS/IDA/GSN station CMLA and of several temporary stations in the Azores archipelago are processed with P and S receiver function (PRF and SRF) techniques. Contrary to regional seismic tomography these methods provide estimates of the absolute velocities and of the Vp/Vs ratio up to a depth of ~300 km. Joint inversion of PRFs and SRFs for a few data sets consistently reveals a division of the subsurface medium into four zones with a distinctly different Vp/Vs ratio: the crust ~20 km thick with a ratio of ~1.9 in the lower crust, the high-Vs mantle lid with a strongly reduced Vp/Vs velocity ratio relative to the standard 1.8, the low-velocity zone (LVZ) with a velocity ratio of ~2.0, and the underlying upper-mantle layer with a standard velocity ratio. Our estimates of crustal thickness greatly exceed previous estimates (~10 km). The base of the high-Vs lid (the Gutenberg discontinuity) is at a depth of ~80 km. The LVZ with a reduction of S velocity of ~15% relative to the standard (IASP91) model is terminated at a depth of ~200 km. The average thickness of the mantle transition zone (TZ) is evaluated from the time difference between the S410p and SKS660p, seismic phases that are robustly detected in the S and SKS receiver functions. This thickness is practically similar to the standard IASP91 value of 250 km, and is characteristic of a large region of the North Atlantic outside the Azores plateau. Our data are indicative of a reduction of the S-wave velocity of several percent relative to the standard velocity in a depth interval from 460 to 500 km. This reduction is found in the nearest vicinities of the Azores, in the region sampled by the PRFs, but, as evidenced by SRFs, it is missing at a distance of a few hundred kilometers from the islands. We speculate that this anomaly may correspond to the source of a plume which generated the Azores hotspot. Previously, a low S velocity in this depth range was found with SRF techniques beneath a few other hotspots.

1. Introduction

Hotspots and the related structures in the mantle are of great interest for the theory of the Earth. Morgan (1971) explained hotspots by plumes rising from the lower mantle, but this hypothesis is disputed (e.g., Foulger, 2007). Some global tomographic models (Montelli et al., 2004) suggest a connection between some hotspots (including the Azores) and low-velocity anomalies near the core-mantle boundary, but these features are at the limit of resolution (van der Hilst and de Hoop, 2005). In most studies the only upper mantle anomalies beneath hotspots are low S velocities at depths less than ~300 km (e.g., Ritsema and Allen, 2003). This is because hotspots originate in the upper mantle (e.g., Foulger, 2007), or, alternatively, the low-velocity conduits connecting the upper mantle with the deeper mantle are transient features or that they are too narrow for seismic detection. Even if the plumes are related to processes in the core-mantle boundary region, their internal structures and paths to the surface can be more complicated than usually thought (Davaille et al., 2005; Kumagai et al., 2008). Another issue is the TZ thickness beneath hotspots: if the hotspots are of deep origin, the related depths of the TZ discontinuities should differ from the standard values. However, the related seismic data are controversial with respect to this issue (e.g., Deuss, 2007; Flanagan and Shearer, 1998; Gu et al., 1998; Lawrence and Shearer, 2006; Tauzin et al., 2008).

Global seismic tomography is notable by a low resolution, and local studies with a higher resolution were undertaken at a few hotspot locations. Perhaps the best examples can be found in Iceland, where regional seismic tomography (e.g., Allen et al., 2002) was complemented by receiver functions (e.g., Shen et al., 1998), and these studies were conducted by a few independent groups. Beneath the southern region of the island there is evidence for a columnar low-velocity body with a diameter of ~200 km which extends into the TZ. The 410-km discontinuity within this body is depressed by ~15 km (Shen et al., 1998), whilst the 660-km discontinuity is flat (Du et al.,

* Corresponding author. Instituto Dom Luiz, Campo Grande, Edificio C8, 1749-016 Lisboa, Portugal. Tel.: +351 217500812; fax: +351 217 500 807.
E-mail addresses: mdsilveira@fc.ul.pt (G. Silveira), vinnik@ifz.ru (L. Vinnik), stutz@ipgp.fr (E. Stutzmann), farra@ipgp.fr (V. Farra), kiselev@ifz.ru (S. Kiselev), immorais@fc.ul.pt (I. Morais).

0012-821X/$ – see front matter © 2010 Elsevier B.V. All rights reserved.
doi:10.1016/j.epsl.2010.08.021

2006). The failure to detect topography on the 660-km discontinuity may have a few reasons, which include the ambient temperature at a depth of 660 km or the effect of two coexisting phase transitions with opposite Clapeyron slopes (Hirose, 2002). The other findings in Iceland include detection of a few discontinuities in the upper mantle and the TZ, with important implications for processes in the hotspot (Vinnik et al., 2005).

In the present study we investigate deep structure of another hotspot in the North Atlantic: the Azores. The Azores differ from most other hotspots by anomalously high concentration of water in erupted basalt and large enrichment in incompatible elements and radiogenic isotope ratios (Asimow and Langmuir, 2003). The archipelago consists of 9 islands which mark the surface expression of a large volcanic submarine plateau (Fig. 1a). Formation of the plateau began ~20 Myr ago and ended ~7 Myr ago (Gente et al., 2003). The plateau is located at the triple junction between the African, Eurasian and American plates. The Mid-Atlantic ridge separates America in the west and Eurasia and Africa in the east.

From gravity data, the thickness of the crust beneath the Azores is around 10 km (Gente et al., 2003). Estimates of crustal thickness from seismic refraction data (Senos and Nunes, 1993; Senos et al., 1980; Steinmetz et al., 1976, 1977) are in a range from 7 km for the Mid-Atlantic Ridge to 12–15 km beneath the islands. According to surface wave data the upper mantle beneath Azores is characterized by a broad negative S velocity anomaly beneath the entire plateau. The anomaly is clear at a depth of 100 km, but it disappears between 200 and 300-km depths (Silveira et al., 2006). Yang et al. (2006) inverted P-wave travel time residuals at a local network of 6 stations and found a low-velocity anomaly with a diameter of ~100 km at a depth of ~400 km to the north-east of Terceira Island. At the base of the mantle beneath the Azores, tomographic models display a 2000–4000 km-wide negative S velocity anomaly. Davaille et al. (2005) interpreted this anomaly as a large thermo-chemical dome originating at the CMB. The anomalous material from the dome may pond in the TZ, and secondary plumes emanating from the TZ may generate the Azores and other hotspots in the North Atlantic. Knowledge of a detailed structure of the TZ is of critical importance for testing this hypothesis.

Our study is based on observations of Ps and Sp converted phases in P and S receiver functions (PRFs and SRFs), respectively. In PRFs multiple reflections from shallow discontinuities interfere with Ps transmitted phases from deep discontinuities, but in SRFs the transmitted Sp phases from deep discontinuities arrive much earlier

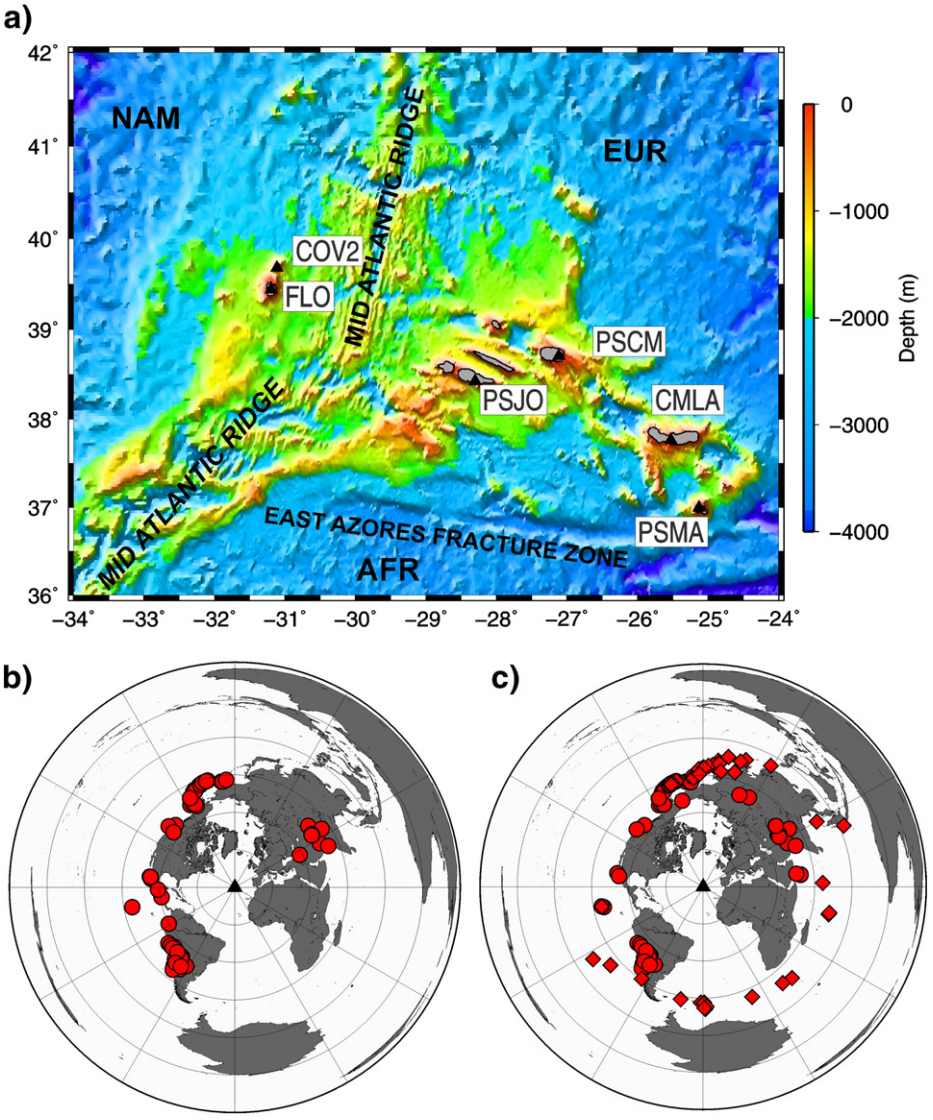

Fig. 1. System of observations: a) Bathymetric map of the Azores with seismograph stations (triangles). NAM, EUR and AFR are the North-American, European and African plates; b) Epicenters of seismic events used for computing PRFs at station CMLA; c) Epicenters of seismic events used at station CMLA for computing S and SKS receiver functions (circles and diamonds, respectively).

than the reverberations. Using S and SKS provides a possibility to sample the same region with two kinds of SRFs. Joint inversion of PRFs, SRFs and teleseismic P and S travel time residuals presents the most efficient way of using them (Vinnik et al., 2004). The experience of joint inversion (e.g., Kiselev et al., 2008; Vinnik et al., 2009) suggests that this approach solves the same structural problems as surface waves, but with higher radial and lateral resolution. Moreover, the joint inversion provides data on both P and S wave velocities (Vp and Vs) and their ratio as a function of depth, which is either difficult or impossible to obtain with other seismic data.

We use recordings of a few temporary stations (FLO, COV, PSJO, PSCM and PSMA) that were deployed between December 2000 and September 2002 in the framework of the COSEA experiment (Coordinated Seismic Experiment at Azores), but most of our data come from IRIS/IDA/GSN station CMLA. The study region is surrounded by earthquake epicenters at appropriate epicentral distances (Fig. 1b, c).

2. P receiver functions

P receiver functions (PRFs) are obtained following Vinnik (1977). For the sketch of the ray paths and the coordinate system see Fig. 1-S of Supplementary Material. The record is represented by the particle motion projections on the axes *L* and *Q*. Axis *L* is parallel to principal P wave particle motion direction in the wave propagation plane. The angle between the *L* axis and the vertical axis (apparent incidence angle) is determined by the analysis of the related covariance matrix. Axis *Q* is normal to *L* in the same plane and is optimum for observing Ps phases. To equalize recordings of different events, *Q* components are deconvolved by the *L* components of the P waves. For the adopted sign convention upward motion in the Ps phase corresponds to positive discontinuity (with a higher velocity at the deeper side of the discontinuity). To detect the Ps phases from deep discontinuities, the individual *Q* components are stacked with move-out time corrections, which depend on the assumed depth of conversion and the P wave slowness. The adopted reference slowness at which no move-out correction is applied to the PRF is 6.4 s/°. This reference slowness is adopted in other PRF studies. To suppress microseismic noise the records were low-pass filtered with a cut-off period of ~8 s.

For station CMLA we stacked 63 individual PRFs. The distance range is between 56° and 90° with an average of 76.9° (Fig. 1b). The total number of PRFs for all the other stations is 35 and they have azimuthal distribution, broadly similar to that in Fig. 1b; the average epicentral distance is 68.6°. The RMS amplitudes of random noise in the stacks are 0.006 and 0.007 for CMLA and COSEA stations, respectively.

The crustal phase, labeled 'C' at a time of ~2 s is well seen in all stacks (Fig. 2). The stack for CMLA (Fig. 2a) displays a large M-shaped phase labeled 'M' with a time of 52.5 s for the dominant negative motion. The amplitude of this phase (~0.1) is many times larger than

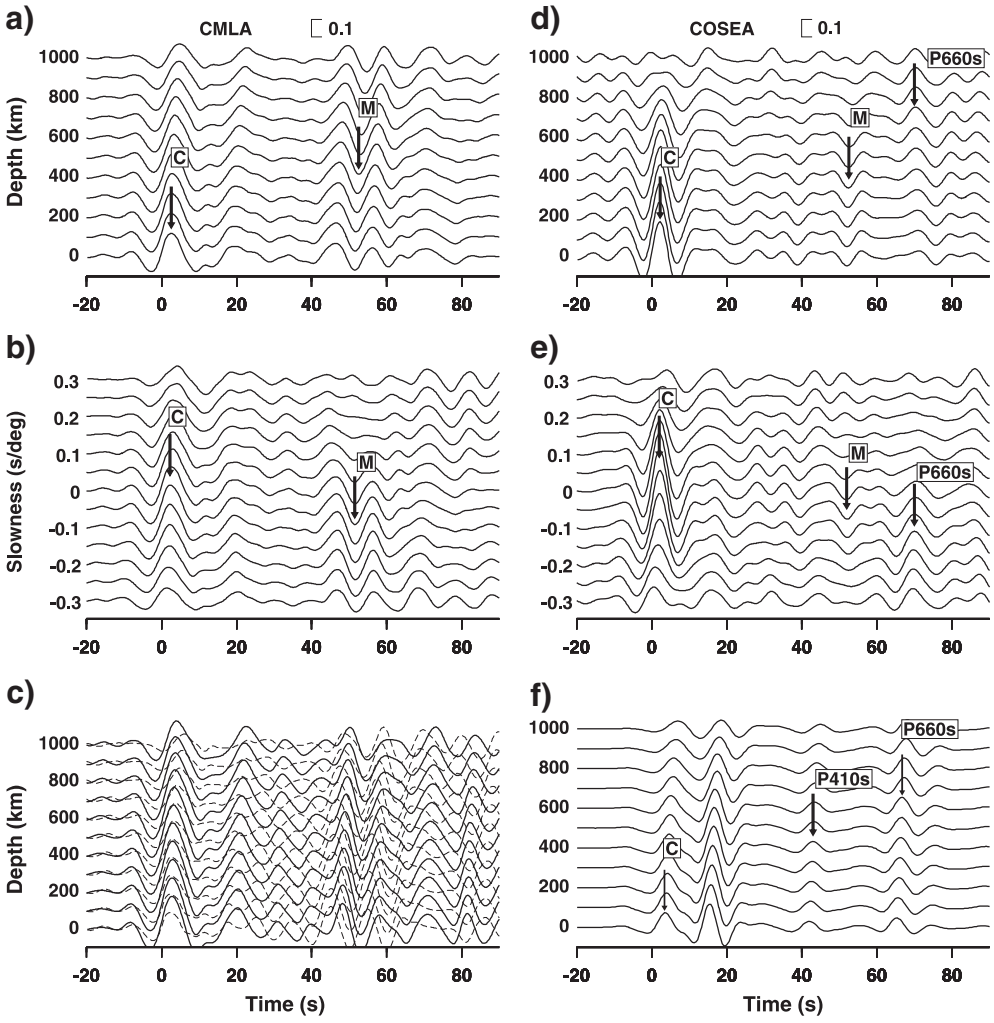

Fig. 2. Stacked PRFs from CMLA (a–c) and COSEA stations (d,e). Synthetic PRFs for IASP91 model (Kennett and Engdahl, 1991) are stacked in (f). In (a, c, d, f) each trace corresponds to the trial depth in km shown on the left-hand side. In (b,e) each trace corresponds to the differential slowness attached on the left-hand side. The arrivals of distinct seismic phases are marked by arrows attached to the traces with the largest amplitudes. In (c) the PRFs from station CMLA are divided into two groups with different back azimuths and stacked separately. Sector West – solid lines; Sector North – dashed lines.

the RMS value of noise. Its waveform is very different from the P410s phase that is expected to arrive in the standard Earth (Fig. 2f). Moreover, the amplitude of the M-shaped phase is at least two times the maximum amplitude of the P410s phase that was ever seen in actual seismograms or in the synthetics for standard models.

Beyond the Ps phases from deep discontinuities the stack may contain reverberations (multiple reflections from shallow discontinuities). To distinguish between reverberations and the Ps phases, another method of stacking can be useful (Andrews and Deuss, 2008; Chevrot et al., 1999). In this method the move-out corrections for stacking are calculated as product of the trial differential slowness (difference between the assumed slowness and the P wave slowness) and the differential distance (difference between the epicentral distance of the seismic event and the average or reference distance of the group of events). The reverberations and the Ps phases should be located in the positive and negative differential slowness ranges, respectively. Application of this method to the CMLA receiver functions (Fig. 2b) indicates that the M-shaped phase is the Ps phase or a result of interference of a few Ps phases.

To judge on possible azimuthal effects in the recordings of the M-shaped phase we divided the set of receiver functions of CMLA into two subsets. One subset corresponds to the back azimuth sector between 210° and 280° ('West'), and the other includes all remaining events ('North'). For the locations of epicenters see Fig. 1b. The M-shaped phase is present in both azimuths but with a relative phase shift of 2 s (Fig. 2c) which is indicative of lateral heterogeneity. Stacking the receiver functions irrespectively of the azimuth minimizes the effect of this heterogeneity.

A similar signal with a strongly dominant negative peak is detected at the same time (52.5 s) in the stack for COSEA stations (Fig. 2d). In the slowness stack (Fig. 2e) this signal is in the negative differential slowness range, which is indicative of the P to S conversion rather than reverberations. The only significant difference between the signals in the CMLA and COSEA data is in the amplitude: −0.064 at COSEA versus −0.1 at CMLA. The smaller amplitude at COSEA still is many times larger than the RMS of random noise. The other phase in the COSEA receiver functions that arrives at a time of 70.1 s, in the slowness stack is in the negative differential slowness range. This is the P660s phase from the bottom of the TZ. The IASP91 (Kennett and Engdahl, 1991) time of this phase is 68 s, and in our seismograms it arrives ~2 s later. The other arrivals that can be recognized in the COSEA stack are either in the positive differential slowness range or their slowness is uncertain, and association of them with the Ps converted phases is not warranted by the available data.

The region where the P phases are converted into S is shown by the surface projections of the piercing points (Fig. 3a). Piercing point is cross-over of the ray-path and the respective discontinuity. Both P410s and P660s piercing points are located beneath the Azores plateau or close to it. The piercing points of the Ps phases comprising the M-shaped signal in Fig. 2 are located between those of P410s and P660s. The first Fresnel zone at a depth of 500 km and at a period of 10 s is nearly circular with a radius of 170 km.

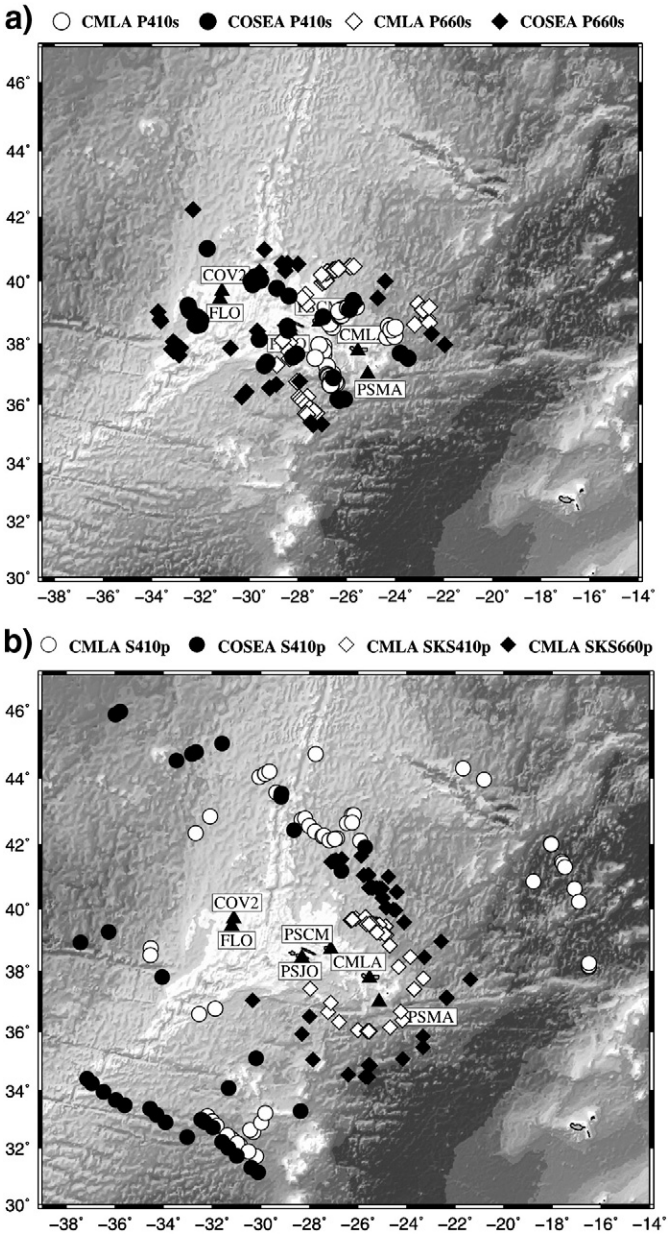

Fig. 3. Surface projections of piercing points of P410s and P660s (a) and S410p, SKS410p and SKS660p (b).

3. S receiver functions

SRF consists mostly of Sp converted phases. In this technique (Farra and Vinnik, 2000) the recording of the S wave train is decomposed into *Q*, *L*, and *M* components. For the sketch of the coordinate system see Fig. 2-S of Supplementary Material. The *Q* and *L* components here are defined differently from those of PRFs. The *Q* axis is parallel to the principal S-wave-particle-motion direction in the wave propagation plane. The *L* axis is normal to *Q* in the same plane. The *L* component is not distorted by the S wave motion and, for this reason, is optimum for detecting the Sp converted phases. The *M* axis is parallel to the principal S wave motion direction in the wave-front plane. This direction depends on the focal mechanism of the seismic event. The directions of all axes are determined from the analyses of the related covariance matrices. The *L* components of a number of seismic events are equalized by deconvolving them by the corresponding *M* components. Opposite to the PRFs, negative polarity of the Sp converted phase corresponds to positive discontinuity (with a higher S velocity on the deeper side of the discontinuity). To suppress noise, the deconvolved *L* components of a number of seismic events are stacked with weights. The weight depends on the angle between the axes *M* and *Q* and on the noise amplitude in the individual *L* component. The procedure involves evaluation of the RMS amplitude of noise σ in the stack. The resulting estimate of σ is close to that given by bootstrap resampling (Vinnik and Farra, 2007).

The Sp phase has a larger slowness than the parent S phase in the same recording. To account for this difference in slowness, the individual receiver functions should be stacked with move-out time corrections that can be calculated accurately with ray theory. However, the Sp phases are often observed at a relatively small distance where they should not exist in ray theoretical limit. To circumvent this problem, we apply slant stacking of the S receiver

functions and calculate the correction as product of the difference in slowness between the Sp phase and S (differential slowness) and the difference between the epicentral distance of the seismic event and the reference distance (differential distance). The detected signal is always seen in the traces corresponding to several values of differential slowness, and its arrival time can vary between the traces. This variability introduces some uncertainties in the estimates of the travel time, and it should be minimized. The dependence of the arrival time on differential slowness means that the average signal amplitude differs between the negative and positive differential distance. We select the reference distance (the distance at which the move-out corrections change their sign) by trial and error and require that the dependence of the arrival time of the Sp phase of interest on the differential slowness is minimal.

To construct SRFs with the optimum signal/noise ratio the row records were low-pass filtered. The cut-off period of the filter varied depending on the spectra of signals and noise, but on the average it was around 0.1 Hz and the dominant period of the filtered S varied within ± 0.02 Hz. For CMLA we obtained SRFs separately for the S phase in a distance range between 65° and 88° and for the SKS phase at larger distances. For the COSEA stations we obtained SRFs only for S. The stack for the S phase at CMLA (Fig. 4a) is obtained from 72 individual SRFs with the average epicentral distance of 78.6° and the reference distance of 79.0°. Two main phases in the stack are the crustal phase at a time near −3 s, and the S410p phase at a time of −57.1 s. The amplitude of S410p (0.036) is 4.5 times the RMS amplitude of noise (0.008). The maximum amplitude is observed at a differential slowness of 0.8 s/°, close to the theoretical value of 0.6 s/°. This S410p arrives 2.6 s earlier than predicted by IASP91 standard model (Kennett and Engdahl, 1991) (see Fig. 4d). The stack of 36 SRFs of COSEA stations (Fig. 4b) contains the same phases. S410p is detected at a time of −61.5 s with the residual of −4.0 s, but this value is relatively unreliable, because the signal amplitude (0.015) is comparable with the RMS amplitude of noise (0.009). The amplitude of S410p at CMLA is close to that observed at many other stations elsewhere, whilst in the stack for the COSEA stations it is anomalously small.

Residuals of time of S410p of comparable magnitude were observed at seismograph stations in California (Vinnik et al., 2010), and it has been shown that a negative residual requires an increased Vp/Vs ratio or a depressed 410-km discontinuity or both. A residual of −2 s can be explained by a Vp/Vs ratio of 1.9 versus ~1.8 in IASP91 in an upper mantle layer 125 km thick or by a depression of 15 km of the 410-km discontinuity or both, but with a smaller magnitude. As will be shown in Section 4, the depression on the 410-km discontinuity is unlikely for the region outside the Azores plateau and then the anomalous velocity ratio presents the only viable alternative.

The anomalous zone in the TZ, evidence of which is found in the PRFs should appear in the SRFs as an anomalous phase arriving several seconds earlier than S410p, but evidence of this phase in Fig. 4a and b is missing. There can be two main reasons for this. The piercing points of S410p are at a distance of several hundred kilometers from the stations, mostly far outside the Azores plateau (Fig. 3b), whilst the piercing points at a depth of ~500 km are at larger distance from the stations than those of S410p. The first Fresnel zone at a period of 10 s is elliptic with a half-length of the axis of either 900 km or 350 km for the wave-propagation plane and perpendicular plane, respectively. It is possible that the anomalous signal from a depth of ~500 km is not detected in SRFs, because the anomaly is located beneath the Azores plateau and vanished outside the plateau. There is another possible reason: the amplitudes of the Sp phases that are generated at a depth of ~500 km are too small for a detection at epicentral distances less than 80°. To check this, we calculated a stack of 30 SRFs from CMLA with the average epicentral distance of 85°. In this stack (not shown) the S410p amplitude (0.039) is 3 times the RMS amplitude of noise, but the anomalous phase is not seen. This result suggests that the anomalous phase is not detected in the SRFs because the anomaly vanished outside the Azores plateau.

The stack of SRFs from CMLA for the SKS phase (Fig. 4c) requires a special discussion. In the SRFs in Fig. 4a and b there is no evidence of the Sp converted phase from the 660-km discontinuity. This is caused by the large slowness of S (more than 9.0 s/°), whilst S660p is efficiently generated only at a smaller slowness that is characteristic of SKS. We stacked 53 SRFs for SKS, almost all of them from station CMLA. The average distance of seismic events is 97.5°, the reference

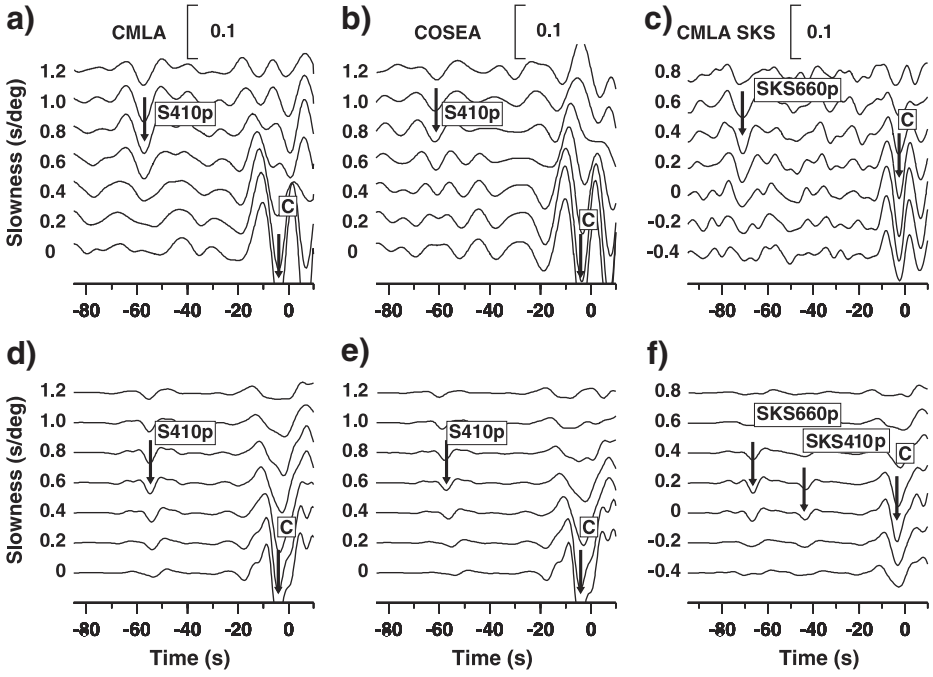

Fig. 4. Stacked SRFs from station CMLA (a), COSEA stations (b) and SKSRFs from CMLA (c). The corresponding synthetic SRFS for IASP91 model are shown in (d–f). Each trace corresponds to the differential slowness shown on the left-hand side. The arrivals of distinct phases are marked by arrows on the traces with the largest amplitudes.

distance is 95°, and the average slowness is 5.2 s/°. The RMS of noise is sufficiently low (0.008), but we do not see in this stack evidence of SKS410p or any other phase related to the TZ, except SKS660p at a time of −71.0 s. Its amplitude is 0.035 which is ~4 times the RMS amplitude of noise. The largest amplitude of the signal is observed at a differential slowness of 0.2 s/°, close to the theoretical estimate (see Fig. 4f). The time of this phase for IASP91 is −66.3 s, and the residual is −4.7 s. Observations of S410p and SKS660p can be used jointly to evaluate the difference in depths between the two discontinuities. A large difference in slowness between these two phases requires an accurate evaluation of the upper mantle velocity model. This subject will be treated in Section 4.

The data in Fig. 4c provide no evidence of either SKS410p or the SKSp phase, equivalent to the M-shaped phase in the PRFs. The piercing points of P410s and P660s for CMLA (Fig. 3a) are not very far from those of SKS660p in Fig. 3b. Some piercing points of the M-shaped phase in the P receiver functions and those of the equivalent phase in the SKS receiver functions should be not very far as well. The first Fresnel zone of the SKS-to-P conversion at a depth of 500 km and at a period of 10 s is elliptic with the half-length of the axis of either 260 km or 230 km for the wave-propagation plane and the perpendicular plane, respectively. The only feasible explanation for the failure to detect both SKS410p and the anomalous signal from a depth of ~500 km is a strong lateral heterogeneity of the upper TZ in the vicinities of CMLA. Evidence for this heterogeneity is clear in Fig. 2c. The TZ can be highly heterogeneous in this area, because it is located near the eastern edge of the Azores plateau.

4. Velocity models

In this Section we consider several interconnected problems. In Section 4.1 we present data on azimuthal anisotropy in the upper mantle beneath station CMLA. In case of strong anisotropy, it should be taken into account in the search for the optimum velocity model of the upper mantle. In Section 4.2, we determine P-wave and S-wave velocity models for the 300 upper kilometers using an algorithm devised for isotropic media. In Section 4.3, we evaluate the TZ thickness, i.e. the difference in depths of the 410-km and 660-km discontinuities, from the travel-times of the S410p and SKS660p seismic phases. These phases are strongly different in slowness (~10 s/° and ~5 s/°, respectively), and to evaluate the thickness of the TZ, accurate P and S velocity profiles for the mantle over the 410-km discontinuity are required. These models are obtained in Section 4.2. Finally in Section 4.3, we construct the S-velocity profile of the TZ that explains the anomalous M-shaped phase in the PRFs.

4.1. Search for azimuthal anisotropy in the upper mantle

To evaluate azimuthal anisotropy in the vicinity of station CMLA we processed collectively 82 recordings of the SKS seismic phases following the method of Vinnik et al. (1984). This method exploits the phenomenon of shear-wave splitting in anisotropic media and is useful in the analysis of noisy recordings from many azimuths. For locations of the corresponding seismic events see Fig. 1c. We equalize the transverse (T) components of SKS by deconvolving them by the respective radial (R) components. The T components thus pre-processed are stacked with weights that depend on the back azimuths of seismic events:

$$F(t,\psi)=\frac{\sum_i T_i(t)\cos(2\varphi_i+\psi)}{\sum_i[\cos(2\varphi_i+\psi)]^2}$$

where t is time, φ_i is back azimuth of the i-th seismic event and ψ is a parameter which varies in a range from 0 to 180°. Assuming that the recordings are narrow-band with the angular frequency ω, $F(t,\psi)$ can be presented for any fixed ψ approximately as

$$F(t,\psi)\approx A(\psi)\ \omega\ \ \delta t\ sin(\omega t),$$

where δt is the delay of the slow split wave relative to the fast one, and $A(\psi)$ is the coefficient that depends on ψ. The maximum value of A is 0.5, and the maximum value of $F(t,\psi)$ is $0.5\omega\ \delta t$. The dependence of $F(t,\psi)$ on $\sin(\omega t)$ implies a quarter-period phase shift between the R and T components of SKS, which presents the major diagnostic property of azimuthal anisotropy.

In our data the maximum value of $F(t,\psi)$ is 0.067 (see Fig. 3-S of Supplementary Material), ω is 0.45rad/s and the related δt is 0.3 s. However, $F(t,\psi)$ in our data is proportional not to $\sin(\omega t)$ but to $\cos(\omega t)$. This means that the T components of SKS in our data are formed not by anisotropy, but by noise of various origins. Since the anisotropy-related T components in our data are much weaker than the actual T components, the true δt is much smaller than 0.3 s, and hence the mantle beneath CMLA is practically isotropic. Previously the conclusion on isotropy of the upper mantle beneath the Azores was obtained by Kuo and Forsyth (1992) from the analysis of analogue recordings. Our result is similar, in spite of a larger number and a higher quality of the available digital recordings.

4.2. Joint inversion of PRFs and SRFs for velocity models

Our technique of inversion was described and tested in the studies of the Tien Shan, Indian shield, Himalaya, Ladakh, Tibet and southern Africa (e.g., Kiselev et al., 2008; Vinnik et al., 2009). We assume that the Earth in the vicinity of the station is laterally homogeneous and isotropic. The result of Section 4.1 justifies the assumption of isotropy. To generate synthetic receiver functions that are compared with the actual receiver functions we use the Thomson–Haskell matrix formalism (Haskell, 1962) for plane waves and plane layers. To apply this algorithm to the spherical Earth we use Earth flattening transformation (Biswas, 1972). The model is defined by velocities Vp, Vs, thickness and density of each layer. Density is derived from Vp by using Birch law. The assumption of plane waves implies that the apparent velocities of all phases are similar. The actual apparent velocities of the S wave and the Sp converted phase can be very different, if the depth of conversion is large, but this effect is generally negligible if the depth of the discontinuity is not more than ~350 km and the period of waves is in a range of ~10 s.

We conduct a search for the optimum models by using an interactive algorithm, similar to Simulated Annealing (Mosegaard and Vestergaard, 1991), from 4 randomly selected starting points. For each starting point we tested up to 10^5 models until they converged to those, which provide a small misfit between the synthetics and the actual receiver functions. Distribution of the model parameters near the misfit minimum is evaluated following Tarantola (2005). We divide the parameter space into cells, and present the results of the search near the misfit minimum by a number of hits in each cell. This number is shown with a color code. A similar statistics is obtained for the data space. The trial models consisted of 4 layers in the crust and 5 layers in the mantle. The search was conducted for a broad range of P and S velocities. The layer thickness could be up to 50–70 km in the mantle and up to 10–30 km in the crust. For the depth of 300 km and more the velocities were fixed at IASP91 values.

A simple theoretical exercise demonstrates that SRFs and PRFs are complementary and their joint inversion is potentially more efficient than separate inversions. Calculations of the receiver functions involve measurements of the apparent incidence angles i_p and i_s of the P and SV waves, respectively. These angles are used as an input in

the inversion procedure. For the homogeneous half-space i_p depends only on Vs via the relation (e.g., Svenningsen and Jacobsen, 2007):

$$\sin\left(\frac{i_p}{2}\right) = pV_s$$

where p is P wave slowness. For the incoming SV, we consider the angle $e_s = 90 - i_s$ and obtain the relation (modified from Savarensky and Kirnos, 1955):

$$tg(e_s) = \frac{2V_s^2 p}{2V_s^2 p^2 - 1}\sqrt{V_p^{-2} - p^2}$$

Thus, contrary to i_p which depends only on Vs, i_s depends on both Vs and Vp, and, if inverted jointly, i_p and i_s constrain both Vp and Vs. The Vp/Vs ratio is also constrained by the travel-times of crustal and upper-mantle multiples (e.g., Zhu and Kanamori, 2000) and by P and S travel-time residuals (see below).

The non-uniqueness of the joint inversion of PRFs and SRFs can be reduced by using the teleseismic S and P traveltime residuals dT_S and dT_P on the assumption that the residuals are generated in a depth range of the unknown model parameters (less than ~350 km). This assumption is based on numerous reports (e.g., Grand, 2002) that the largest lateral P and S velocity variations are found in the upper 300 km of the Earth. The required residuals are absolute, i.e. determined with respect to a velocity model, in our case, IASP91. The residuals dT_S and dT_P can be evaluated from the travel time residuals of the P410s and P660s phases in PRFs. This method is based on the fact that in most regions of the Earth the difference in the arrival times of P660s and P410s (23.9 s) is nearly constant and similar to that of IASP91 (Chevrot et al., 1999). As the 410-km and 660-km discontinuities are related to phase transitions with opposite Clapeyron slopes (Ito and Takahashi, 1989), a coherent uplift or subsidence of them are unlikely, and a constant difference in the arrival times and, hence, depths, implies that the depths are constant. Then the P410s residual can be presented as the difference between dTs and dTp, and they can be evaluated by adopting a realistic ratio between them. This relation is approximate, because we neglected the difference in length of the P and S wave paths as a second-order effect. For the pyrolite mantle composition, variations of the temperature lead to the theoretical dTs/dTp ratio of 2.7, but most of the actual values are in a range from 3.0 to 4.0 (e.g., Vinnik et al., 1999).

P410s at our stations cannot be detected with confidence, and for the residual of P410s we assumed plausible values. We inverted SRFs and PRFs without the residuals (a) and with the residuals (b,c,d). For the residual of P410s we adopt 3.0 s, obtained by Du et al. (2006) for the peripheral regions of Iceland: in these regions the difference between P660s and P410s arrival times is close to the standard value, which implies the standard depth of the 410-km discontinuity. If the dTs/dTp ratio is 4.0, dTs and dTp are 4.0 s and 1.0 s respectively (case b). If this ratio is 3.0, dTs and dTp are 4.5 s and 1.5 s (case c). We also adopted a smaller P410s residual (2.0 s) and a ratio of 3.0. The resulting dTs and dTp are 3 s and 1 s, respectively (case d). As will be shown, the differences in the adopted residuals lead only to second-order differences in the resulting models.

The inversions for station CMLA (Fig. 5) demonstrate that the velocity model can be divided into four major zones: 1 — the crust at depths from 0 to 20–30 km with a Vp/Vs velocity ratio in the lower crust much higher than the standard ratio of 1.7; 2 — the high-S-velocity (~4.4 km/s) mantle lid at depths from 30 km to 70–80 km with a velocity ratio much lower than the standard ratio of 1.8; 3 — the low-S-velocity (~3.7 km/s) zone (LVZ) with a velocity ratio of ~2.0, terminated at a depth of 150–200 km, and 4 — the underlying upper-mantle layer with a standard velocity ratio. The Vp/Vs anomalies in the crust and the high-velocity mantle lid are present in the models obtained without the residuals (a) and with the residuals (b–d). The Vp/Vs anomalies in the LVZ are seen only in the models with the residuals. Another difference between the models in Fig. 5a and (b–d) is in a width of the bands of acceptable velocity models. For CMLA station, very similar models are obtained from the inversion of PRFs and SKSRFs, instead of SRFs (Fig. 6). A sharp boundary between the high Vp/Vs-ratio crust and the low Vp/Vs-ratio mantle lithosphere is found at a depth of ~20 km. The boundary between the high velocity mantle lid and the LVZ (Gutenberg discontinuity) is at a depth of 80 km. Qualitatively, similar models are also obtained by inversion of PRFs and SRFs from COSEA stations (Fig. 7). A high Vp/Vs ratio in the crust is not evident in Fig. 7, but the transition to the low Vp/Vs-ratio mantle layer at a depth of 30 km is clear. The similarity between the models in Figs. 5–7 obtained for various input data suggests that these models are robust. Note that the Sp phase from the Gutenberg discontinuity is well seen in the SRFs at a time of −10 s (Fig. 4a, b), but it is not seen in the PRFs (Fig. 2), owing to interference with crustal multiples.

To test robustness of the Vp/Vs anomalies in Figs. 5–7 we conducted modeling experiments. A typical result is shown in Fig. 8. One of the S velocity profiles from Fig. 5 was complemented by the P velocity profile with the Vp/Vs ratio from IASP91 model. Density was derived from the P velocity by using Birch law. The synthetics for this model were summed with 7% random noise and the related receiver functions were inverted like the actual receiver functions. In the models obtained with or without the residuals there are no Vp/Vs anomalies, comparable to those in Figs. 5–7. We conclude that the anomalies in Figs. 5–7 are not processing artifacts. Fig. 8 also illustrates the role of travel time residuals in the inversion. For the inversion without the residuals, the residuals of the obtained models are scattered in a range of a few seconds. This range is sharply reduced in the models constrained by the residuals. Accordingly, the bands of the acceptable Vp, Vs and Vp/Vs become more narrow.

4.3. Models of the TZ

The wave-paths of S410p and SKS660p and their lengths in the upper mantle are very different. Therefore, to evaluate the thickness of the TZ from the difference in travel times of S410p and SKS660p, an accurate upper mantle velocity model is required. For the depths from the surface to 350 km we use the model (Fig. 9), consistent with the models in Figs. 5–7. IASP91 model is adopted for larger depths. This model predicts the times of S410p and SKS660p at CMLA as −56.7 s and −70.4 s, respectively. The observed times are −57.1 s and −71.0 s, close to the predicted. The predicted difference in time between S410p and SKS660p is 13.7 s, 0.2 s smaller than the observed time, which suggests that the actual difference in depths between the 660-km and 410-km discontinuities in the study region is slightly (4 km) larger than the standard, given by IASP91. This difference, however, is beyond resolution of our measurements. Sensitivity of this method to the upper mantle model can be demonstrated by an example, where the model in Fig. 9 is replaced by IASP91. The resulting times of S410p and SKS660p are −54.04 and −66.35 s, respectively, and the difference between them is 12.3 s, 1.4 s less than for the model in Fig. 9.

We modeled the anomalous M-shaped phase in PRFs (Section 2) by trial and error. The synthetics were generated by using reflectivity techniques (Fuchs and Mueller, 1971). For the upper 350 km we adopt a model, similar to that in Fig. 9. The parameters of the 410-km discontinuity (depth, Vp, Vs and density) are adopted from IASP91. We try to keep the model in the TZ as close to IASP91, as possible, but numerical experiments testify that it is impossible to obtain the signal with a large negative motion without assuming a low S velocity in the TZ. The synthetic amplitude is sensitive to the S velocity contrast at the negative discontinuity at a depth of 460 km. In our favorite model (Fig. 10) S velocity anomaly at a depth of 460 km is −0.4 km/s, and

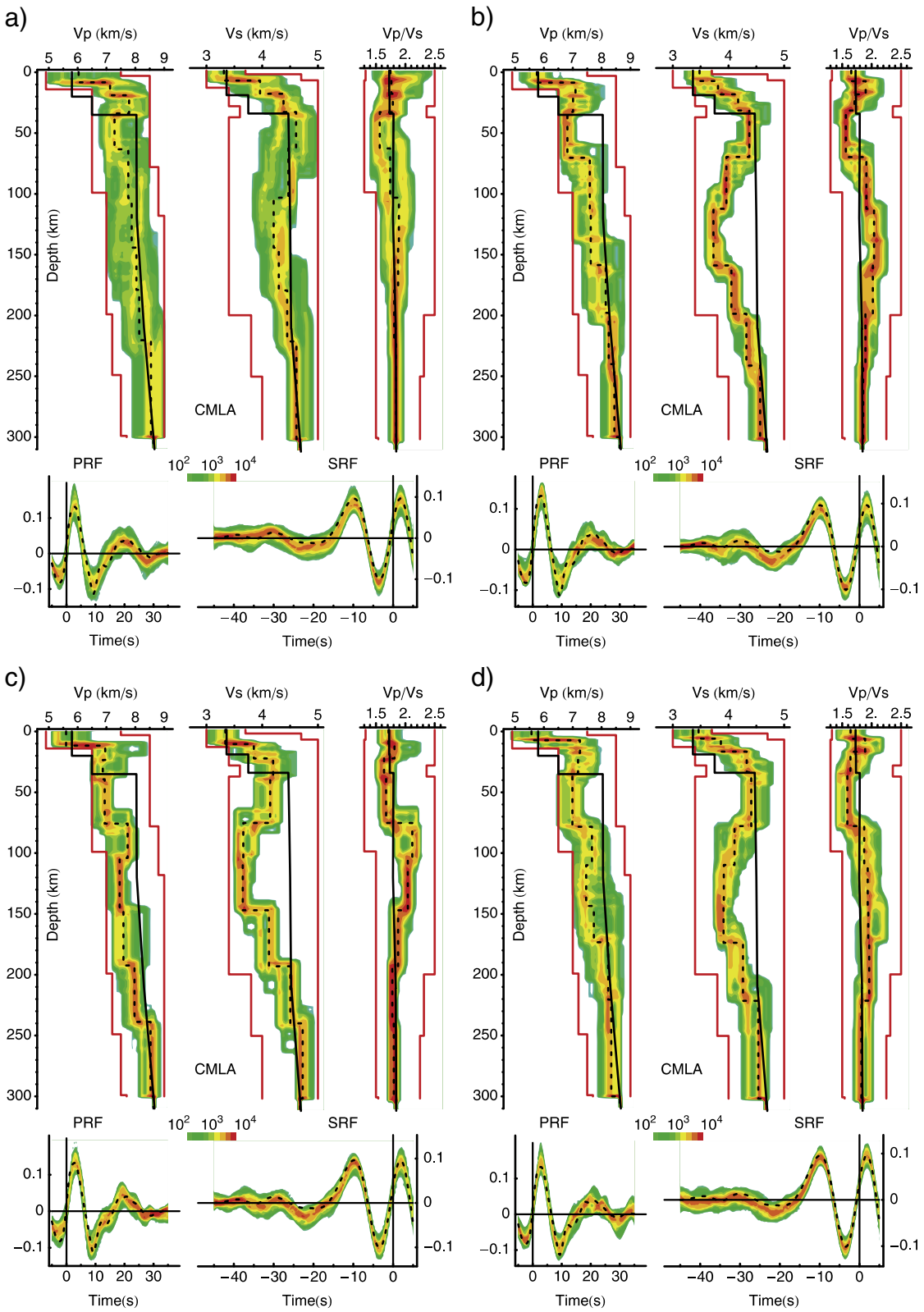

Fig. 5. Joint inversion of PRFs and SRFs from CMLA. Histograms of Vp, Vs and Vp/Vs ratio are shown by color code. Dash lines are for the medians; solid lines are for the IASP91 velocities and their ratios. Red lines are limits of the search. The limits for Vp/Vs are derived from the limits for Vp and Vs: (Vp/Vs)min = (Vp)min/(Vs)max; (Vp/Vs)max = (Vp)max/(Vs)min. Histograms of the synthetic PRFs and SRFs are shown by the same color code as the models; dash lines are for the actual receiver functions. a) inversion without the travel-time residuals; b) dTs = 4.0 s, dTp = 1.0 s; c) dTs = 4.5 s, dTp = 1.5 s; d) dTs = 3.0 s, dTp = 1.0 s.

the resulting waveform is close to the observed waveforms. The synthetic amplitude is larger than at COSEA stations, but the amplitude at COSEA stations is 30% lower than at CMLA. Of course this model is not unique, but the depth and the S velocity contrast of the negative discontinuity are constrained by the time and amplitude of the observed signal.

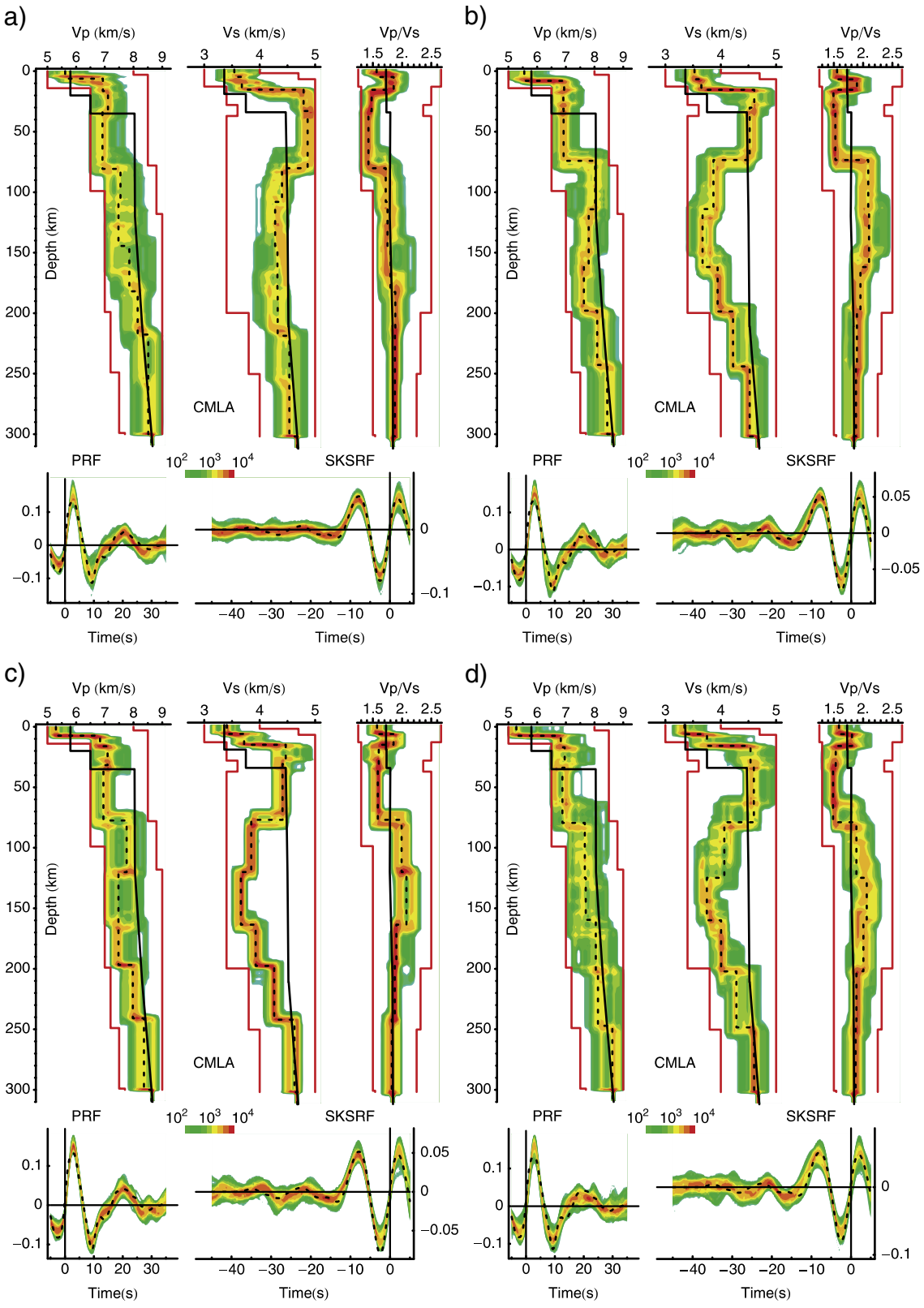

Fig. 6. The same as in Fig. 5, but for SKSRFs instead of SRFs.

5. Discussion and conclusions

We have demonstrated that the joint inversion of the P and S receiver functions constrains not only the S velocity profile to a depth of ~300 km but also the Vp/Vs ratio. The remarkable similarity between the models in Figs. 5–7 from the three data sets implies that our results are robust, at least on a qualitative level. The large difference between the locations of the piercing points of P410s and S410p in Fig. 3 may suggest that P and S receiver functions sample very different regions. However, the major discontinuities in the

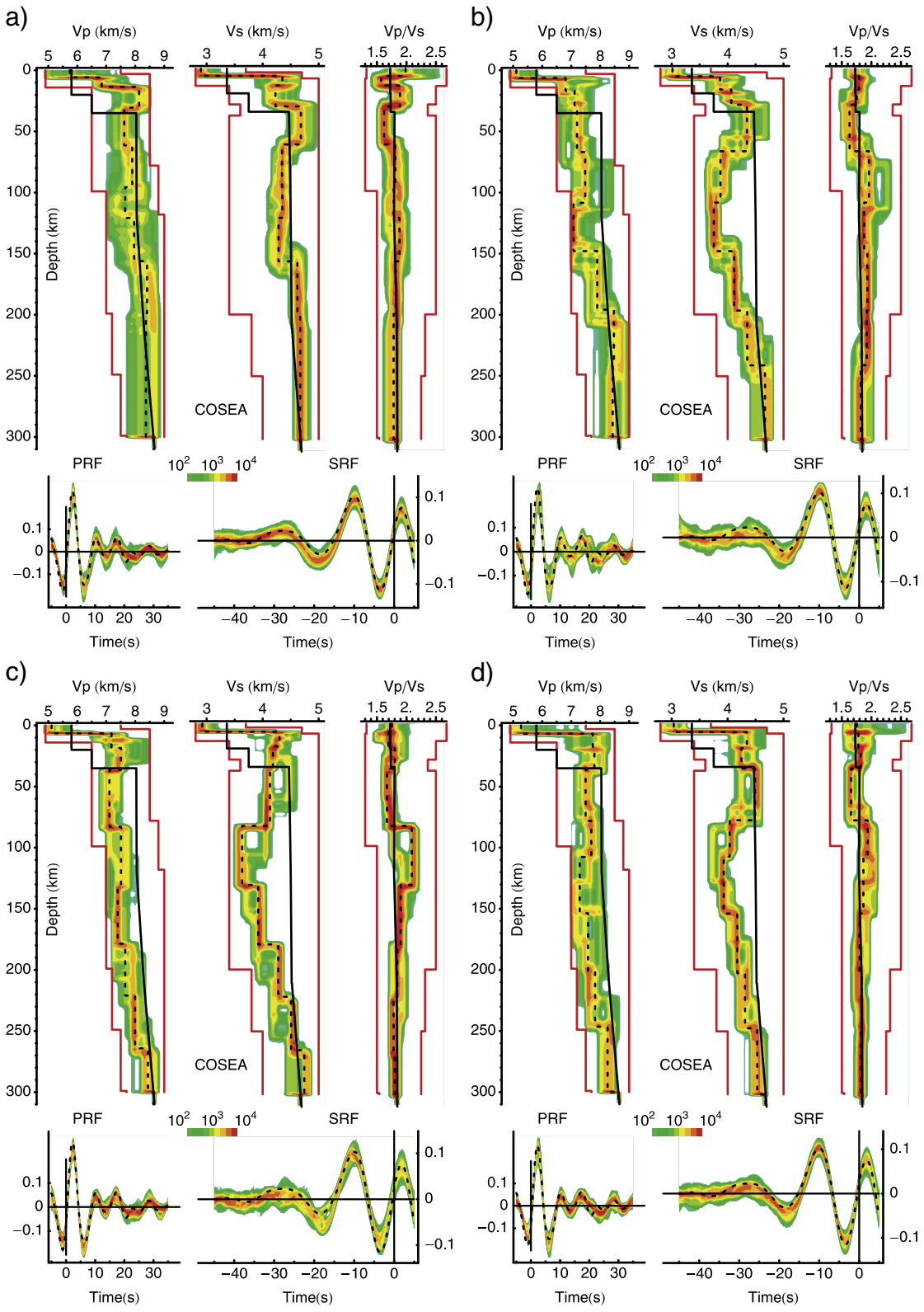

Fig. 7. The same as in Fig. 5, but for COSEA stations.

models are not more than ~80 km deep, and a separation between the piercing points at this depth is ~5 times less than in Fig. 3.

Our data suggest that the lower crust and the uppermost mantle beneath the Azores differ not so much in the absolute wave velocities as in the Vp/Vs velocity ratio. The ratio of 1.8–1.9 is characteristic of mafic crustal rocks like gabbro (e.g., Christensen and Mooney, 1995). The crust thus found is 20–30 km thick, whilst previous estimates for the Azores were around 10 km (see Introduction). The Vp velocity profiles in Figs. 5–7 contain a large discontinuity at a depth of ~10 km, which in P refraction experiments can be taken for the Moho. The equivalent S velocity boundary is at a depth of ~20 km, and the Vp/Vs ratio in the layer

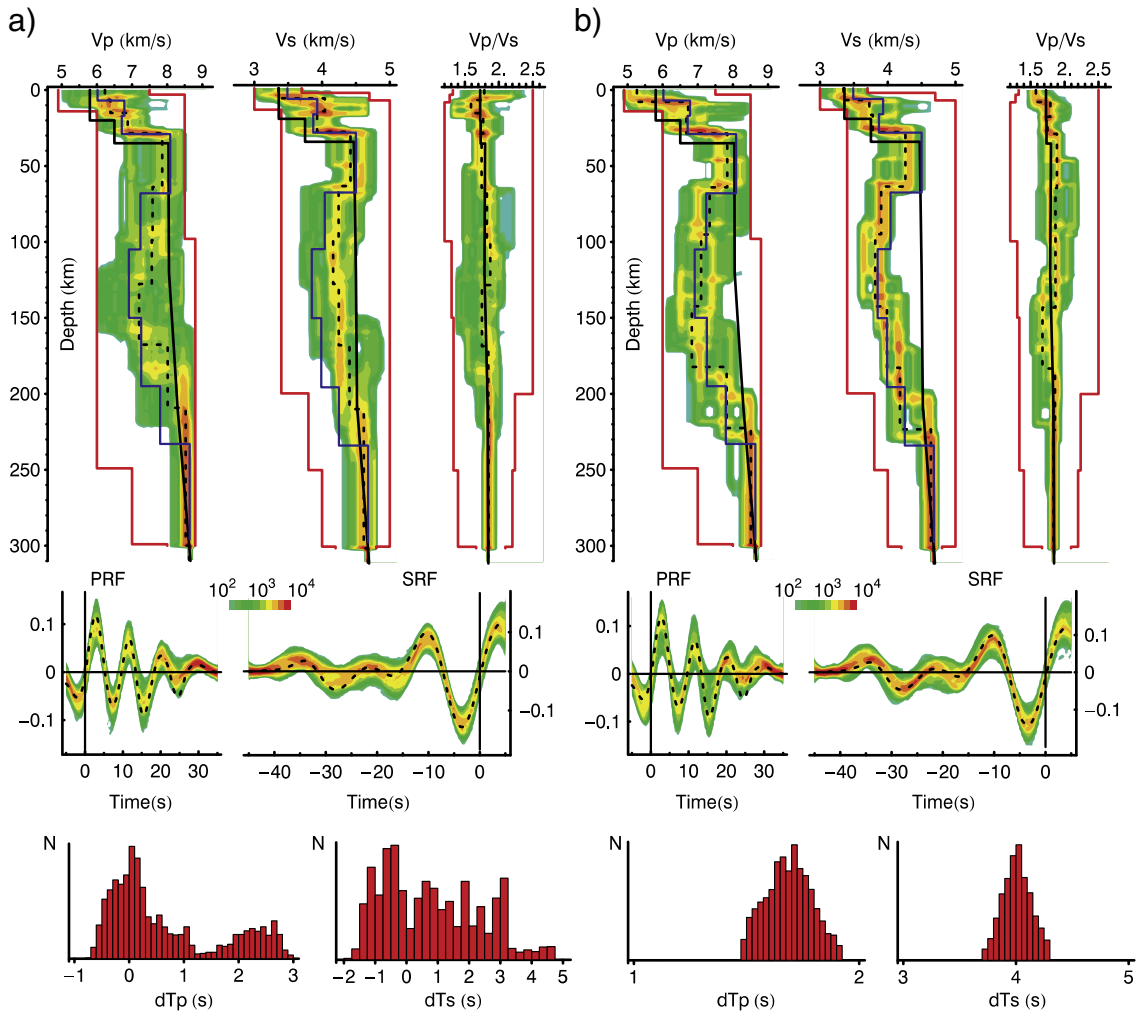

Fig. 8. Examples of joint inversion of synthetic PRFs and SRFs. The inversions with and without teleseismic travel time residuals are shown on the right-hand and left-hand sides, respectively. The residuals are 1.7 s and 4.0 s for the P and S waves, respectively. The Vp, Vs and Vp/Vs used for computing the synthetics are shown by blue lines. Histograms of Vp, Vs and Vp/Vs ratio are shown by color code. Dash lines are for the medians; black solid lines are for the IASP91 velocities and their ratios. Red lines are limits of the search. Histograms of the synthetic PRFs and SRFs are shown by the same color code as the models; dash lines are for the actual receiver functions. Histograms for the travel time residuals are shown at the bottom of the figure.

between 10-km and 20-km depths is anomalously high. This anomalous thickness of the crust is not surprising considering its relation to the large volcanic plateau.

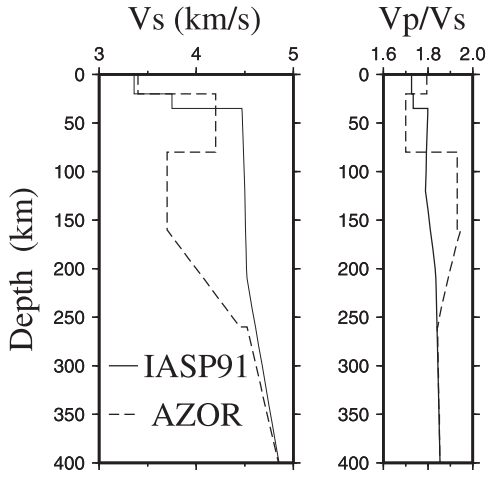

Fig. 9. P and S velocity models used for computing theoretical travel-times of S410p and SKS660p.

In the high-S-velocity mantle lid with a bottom at a depth of 80 km we find a Vp/Vs velocity ratio of 1.6–1.7. Comparable estimates of the lid thickness were obtained for Hawaii (Bock, 1991), the central Pacific (Gaherty et al., 1996), Philippines sea (Gaherty et al., 1999), and Iceland (Vinnik et al., 2005). Harmon et al. (2009) obtained a lower value (60 km) at the fast-spreading West-Pacific ridge. This layer is a residuum formed by depletion of the mantle in water and basaltic component (e.g., Phipps Morgan, 1997). The Gutenberg discontinuity marks the fossilized lower boundary of the melt separation zone that was active during the crust formation (Gaherty et al., 1996). The depth of the melt separation zone depends on temperature, and a comparable depth of the G discontinuity beneath the Azores and other oceanic regions testifies against a large difference in the mantle temperature beneath the Azores and other regions. A large thickness of the crust beneath the Azores suggests that the basaltic component is almost totally removed from the mantle lid. The low Vp/Vs ratio in the high-velocity lid can be controlled by a high content of orthopyroxene, because Vp in orthopyroxene is about 6% lower than in olivine, whilst their S velocities are almost the same (James et al., 2004). The low Vp/Vs ratio can also be a result of a low content of aluminum (Wang et al., 2008) or of vertical transverse isotropy.

The LVZ beneath the G discontinuity is well pronounced in the S wave velocity which is ~15% lower than in IASP91. The Vp/Vs ratio in

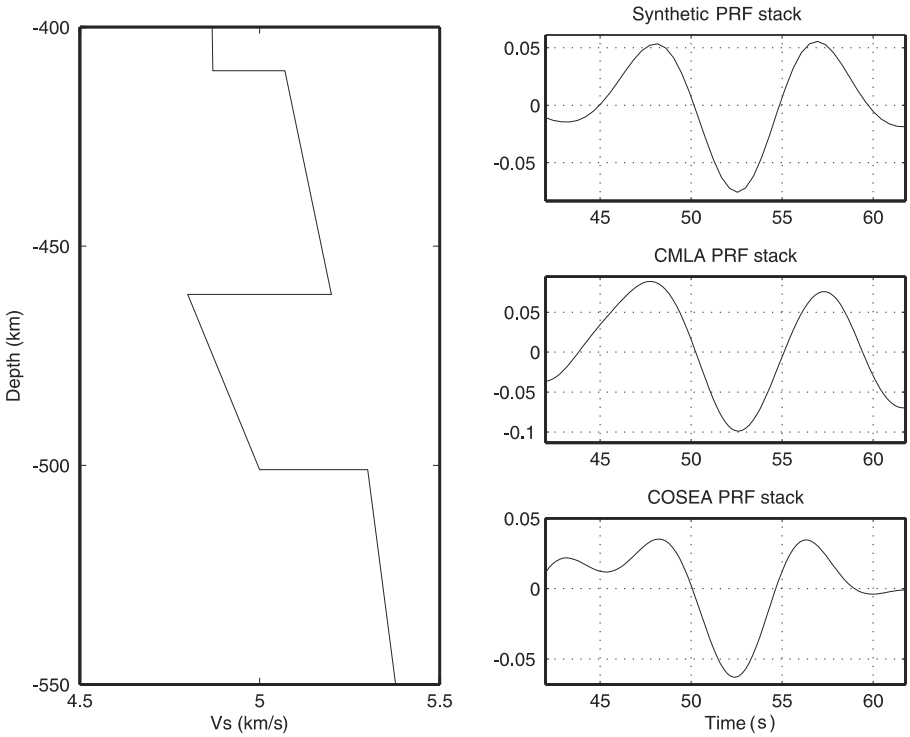

Fig. 10. S velocity profile of the TZ beneath the Azores (left-hand side). The related synthetic Ps phase and the observed Ps phases from CMLA and COSEA stations are shown on the right-hand side.

the LVZ is ~2.0 versus ~1.8 in IASP91 and other global models. The high Vp/Vs ratio is independently indicated by the travel time of S410p. This ratio can be qualitatively explained by melting (Hammond and Humphreys, 2000). The observed S velocity reduction of ~15% at a depth of 100–150 km is ~3 times the model prediction for Iceland (Kreutzmann et al., 2004).

The thickness of the TZ beneath the oceans is a subject of debate with a few studies (e.g., Flanagan and Shearer, 1998; Gu et al., 1998) claiming values less than 240 km. These studies demonstrate a large (up to ~20 km) difference in the TZ thickness beneath Eurasia and North America, which is not found in the studies like Chevrot et al. (1999) or Tauzin et al. (2008). Our analysis provides an independent estimate of this thickness for a large oceanic region that is bounded by piercing points of S410p and SKS660p from station CMLA (Fig. 3). The obtained value of the time difference between S410p and SKS660p yields the standard TZ thickness (~250 km). This estimate corresponds to the region outside the Azores plateau, but we have no data to judge on the depths of the 410-km and 660-km discontinuities beneath the plateau.

Evidence of anomalous structure in the TZ beneath the Azores is a significant result of our study. This result is obtained from the two independent data sets: PRFs from CMLA and from COSEA temporary stations. Indications of anomalous converted and reflected phases in this region, similar to those in our data, can be seen in the data of Deuss (2007) and Tauzin et al. (2008), but the authors left them without any comment. The result of Deuss (2007) is especially important because it is obtained from very different data (precursors to SS). These observations require the presence of a low S velocity layer in the TZ. Previously similar anomalies beneath several hotspots (Afar, Iceland, Cameroon, Baja-Guadeloupe, southern Atlantic) were reported in the studies based only on SRFs (e.g., Vinnik and Farra, 2006; Vinnik et al., 2005, 2009, 2010) and they could be ignored as artifacts of the method, but now a similar structure is found from PRFs. The layer is found only in the nearest vicinity of the islands, sampled by the PRFs, and it is missing at a larger distance, sampled by the SRFs.

A reduced S velocity in the TZ is generally indicative of hydration (Smith and Jacobsen, 2006). A local anomaly of 1 ~ wt.% of water may generate a velocity anomaly of several percent. Anderson (2007) argued that large tomographic variations in the TZ can be created by "low shear velocity of eclogite and its low melting temperature". We note that the low S velocity beneath the Azores and a few other hotspots is found in the same depth range between, approximately, 450 km and 520 km. The low-velocity material may pond at these depths, and generate secondary plumes, in a broad agreement with the ideas of Davaille et al. (2005).

Supplementary materials related to this article can be found online at doi:10.1016/j.epsl.2010.08.021.

Acknowledgments

This is Paris Sorbonne Cite – IPGP UMR 7154 contribution number 3071. We thank IRIS DMC for the recordings of station CMLA and participants of COSEA project for the recordings of the other stations. The authors thank the RLBM for providing one station. This study was partially funded by CV-PLUME project (Ref. PTDC/CTE-GIN/64330/2006). L. Vinnik and S. Kiselev were partially supported by the Russian Fund for Basic Research (RFBR), grant 0705-00315. The authors thank two anonymous reviewers for constructive comments.

References

Allen, R.M., Nolet, G., Morgan, W.J., Vogfjord, K., Bergsson, B.H., Erlendsson, P., Foulger, G.R., Jakobsdottir, S., Julian, B.R., Pritchard, M., Ragnarsson, S., Strefansson, R., 2002. Imaging the mantle plume beneath Iceland using integrated seismological techniques. J. Geophys. Res. 107 (No B12), 2325. doi:10.1029/2001JB000595.

Anderson, D.L., 2007. The eclogite engine: chemical geodynamics as a Galileo thermometer. In: Foulger, G.R., Jurdy, D.M. (Eds.), Plates, Plumes, and Planetary Processes: Geological Society of America. Special Paper, 430, pp. 47–63.

Andrews, J., Deuss, A., 2008. Detailed nature of the 660 km region in the mantle from global receiver function data. J. Geophys. Res. 113, B06304. doi:10.1029/2007JB005111.

Asimow, P.D., Langmuir, C.H., 2003. The importance of water to oceanic mantle melting regimes. Nature 421, 815–820. doi:10.1038/nature01429.

Biswas, N.N., 1972. Earth-flattening procedure for the propagation of Rayleigh wave. Pure Appl. Geophys. 96, 61–74.
Bock, G., 1991. Long-period S to P converted waves and the onset of partial melting beneath Oahu, Hawaii. Geophys. Res. Lett. 18, 869–872. doi:10.1029/91GL01055.
Chevrot, S., Vinnik, L., Montagner, J.-P., 1999. Global scale analysis of the mantle Pds phases. J. Geophys. Res. 104 (B9), 20203–20219. doi:10.1029/1999JB900087.
Christensen, N.I., Mooney, W.D., 1995. Seismic velocity structure of the continental crust: a global view. J. Geophys. Res. 100 (B6), 9761–9788.
Davaille, A., Stutzmann, E., Silveira, G., Besse, J., Courtillot, V., 2005. Convective patterns under the Indo-Atlantic "box". Earth Planet. Sci. Lett. 239, 233–252. doi:10.1016/j.epsl.2005.07.024.
Deuss, A., 2007. Seismic observations of transition-zone discontinuities beneath hotspot locations. In: Foulger, G.R., Jurdy, D.M. (Eds.), Plates, Plumes, and Planetary Processes: Geological Society of America. Special Paper, 430, pp. 121–131.
Du, Z., Vinnik, L.P., Foulger, G.R., 2006. Evidence from P-to-S mantle converted waves for a flat 660-km" discontinuity beneath Iceland. Earth Planet. Sci. Lett. 241, 271–280.
Farra, V., Vinnik, L., 2000. Upper mantle stratification by P and S receiver functions. Geophys. J. Int. 141, 699–712.
Flanagan, M.F., Shearer, P.M., 1998. Global mapping of topography on transition zone velocity discontinuities by stacking SS precursors. J. Geophys. Res. 103 (B2), 2673–2692. doi:10.1029/97JB03212.
Foulger, G.R., 2007. The "plate" model for the genesis of melting anomalies. In: Foulger, G.R., Jurdy, D.M. (Eds.), Plates, Plumes, and Planetary Processes: Geological Society of America. Special Paper, 430, pp. 1–28.
Fuchs, K., Mueller, G., 1971. Computation of synthetic seismograms with the reflectivity method and comparison with observations. Geophys. J. R. Ast. Soc. 23, 417–433.
Gaherty, J.B., Jordan, T.H., Gee, L.S., 1996. Seismic structure of the upper mantle in a central Pacific corridor. J. Geophys. Res. 101 (B10), 22291–22309. doi:10.1029/96JB01882.
Gaherty, J.B., Kato, M., Jordan, T.H., 1999. Seismological structure of the upper mantle: a regional comparison of seismic layering. Phys. Earth Planet. Inter. 110, 21–41.
Gente, P., Dyment, J., Maia, M., Goslin, J., 2003. Interaction between the Mid-Atlantic Ridge and the Azores hot spot during the last 85 Myr: emplacement and rifting of the hot spot-derived plateaus. Geochem. Geophys. Geosyst. 4 (10), 8514. doi:10.1029/2003GC000527.
Grand, S.P., 2002. Mantle shear-wave tomography and the fate of subducted slabs. Philos. Trans. R. Soc. London 360, 2475–2491.
Gu, Y.J., Dziewonski, A.M., Agee, C.B., 1998. Global de-correlation of the topography of transition zone discontinuities. Earth Planet. Sci. Lett. 157, 57–67.
Hammond, W.C., Humphreys, E.D., 2000. Upper mantle seismic wave velocity: effects of realistic partial melt geometries. J. Geophys. Res. 105 (B5), 10975–10986. doi:10.1029/2000JB900041.
Harmon, N., Forsyth, D.W., Weeraratne, D.S., 2009. Thickening of young Pacific lithosphere from high-resolution Rayleigh wave tomography: a test of the conductive cooling model. Earth Planet. Sci. Lett. 278, 96–106. doi:10.1016/j.epsl.2008.11.025.
Haskell, N.A., 1962. Crustal reflection of plane P and SV waves. J. Geophys. Res. 67, 4751–4767.
Hirose, K., 2002. Phase transitions in pyrolitic mantle around 670-km depth: implications for upwelling of plumes from the lower mantle. J. Geophys. Res. 107 (B4), 2078. doi:10.1029/2001JB000597.
Ito, E., Takahashi, E., 1989. Postspinel transformations in the system Mg_2SiO_4–Fe_2SiO_4, and some geophysical implications. J. Geophys. Res. 94 (B8), 10637–10646.
James, D.E., Boyd, F.R., Schutt, D., Bell, D.R., Carlson, R.W., 2004. Xenolith constraints on seismic velocities in the upper mantle beneath southern Africa. Geochem. Geophys. Geosyst. 5, Q01002. doi:10.1029/2003GC000551.
Kennett, B.L.N., Engdahl, E.R., 1991. Travel times for global earthquake location and phase identification. Geophys. J. Int. 105, 429–465.
Kiselev, S., Vinnik, L., Oreshin, S., Gupta, S., Rai, S.S., Singh, A., Kumar, M.R., Mohan, G., 2008. Lithosphere of the Dharawar craton by joint inversion of P and S receiver functions. Geophys. J. Int. 173, 1106–1118. doi:10.1111/j.1365-246X.2008.03777.x.
Kreutzmann, A., Schmeling, H., Junge, A., Ruedas, T., Marquart, G., Bjarnason, I.Th., 2004. Temperature and melting of a ridge-centered plume with application to Iceland. Part II: Predictions for electromagnetic and seismic observables. Geophys. J. Int. 159, 1097–1111.
Kumagai, I., Davaille, A., Kurita, K., Stutzmann, E., 2008. Mantle plumes: thin, fat, successful, or failing? Constraints to explain hot spot volcanism through time and space. Geophys. Res. Lett. 35, L16301. doi:10.1029/2008GL035079.
Kuo, B.-Y., Forsyth, D.W., 1992. A search for split SKS waveforms in the North Atlantic. Geophys. J. Int. 108, 557–574.
Lawrence, J.F., Shearer, P.M., 2006. A global study of transition zone thickness using receiver functions. J. Geophys. Res. 111, B06307. doi:10.1029/2005JB003973.
Montelli, R., Nolet, G., Dahlen, F.A., Masters, G., Engdahl, E.R., Hung, S.-H., 2004. Finite-frequency tomography reveals a variety of plumes in the mantle. Science 303, 338–343. doi:10.1126/science.1092485.
Morgan, W.J., 1971. Convection plumes in the lower mantle. Nature 230, 42–43. doi:10.1038/230042a0.
Mosegaard, K., Vestergaard, P.D., 1991. A simulated annealing approach to seismic model optimization with sparse prior information. Geophys. Prospect. 39, 599–611.
Phipps Morgan, J., 1997. The generation of a compositional lithosphere by mid-ocean ridge melting and its effect on subsequent off-axis hotspot upwelling and melting. Earth Planet. Sci. Lett. 146, 213–232.
Ritsema, J., Allen, R.M., 2003. The elusive mantle plumes. Earth Planet. Sci. Lett. 207, 1–12. doi:10.1016/S0012-821X(02)01093-2.
Savarensky, E.F., Kirnos, D., 1955. Elements of seismology and seismometry. GITTL, Moscow (in Russian).
Senos, M.L., Nunes, J.C., 1993. Constituição da litosfera Atlântica na região das ilhas dos Açores. I.N.M.G, Lisboa (in Portuguese).
Senos, M.L., Nunes, J.C., Moreira, V.S., 1980. Estudos da estrutura da crosta e manto superior nos Açores. I.N.M.G, Lisboa (in Portuguese).
Shen, Y., Solomon, S.C., Bjarnason, I.T., Wolfe, J.C., 1998. Seismic evidence for a lower-mantle origin of the Iceland plume. Nature 395, 62–65. doi:10.1038/25714.
Silveira, G., Stutzmann, E., Davaille, A., Montagner, J.-P., Mendes-Victor, L., Sebai, A., 2006. Azores hotspot signature in the upper mantle. J. Volconol. Geotherm. Res. 156, 23–34. doi:10.1016/j.jvolgeores.2006.03.022.
Smith, J.R., Jacobsen, S.D., 2006. Nominally anhydrous minerals and Earth's deep water cycle. In: van der Lee, S., Jacobsen, S.D. (Eds.), Earth's deep water cycle: American Geophysical Union. Geophys. Monogr. Ser., 168, pp. 1–12. doi:10.1029/168GM02.
Steinmetz, L., Hirn, A., Sapin, M., Whitmarsh, R., Moreira, V., 1976. Zone of P wave attenuation beneath the crest of Mid-Atlantic ridge. Bull. Soc. Géol. Fr. 4 (7), 931–936.
Steinmetz, L., Whitmarsh, R., Moreira, V., 1977. Upper mantle structure beneath mid-Atlantic ridge north of Azores based on observations of compressional waves. Geophys. J. R. Ast. Soc. 50 (2), 353–380.
Svenningsen, L., Jacobsen, B.H., 2007. Absolute S-velocity estimation from receiver functions. Geophys. J. Int. 170 (3), 1089–1094.
Tarantola, A., 2005. Inverse problem theory and methods for model parameter estimation. Soc. Ind. Appl. Math. 342.
Tauzin, B., Debayle, E., Wittlinger, G., 2008. The mantle transition zone as seen by global Pds phases: no clear evidence for a thin transition zone beneath hotspots. J. Geophys. Res. 113, B08309. doi:10.1029/2007JB005364.
Van der Hilst, R.D., de Hoop, M.V., 2005. Banana-doughnut kernels and mantle tomography. Geophys. J. Inter. 163, 956–961.
Vinnik, L., 1977. Detection of waves converted from P to SV in the mantle. Phys. Earth Planet. Inter. 15, 39–45.
Vinnik, L., Farra, V., 2006. S velocity reversal in the mantle transition zone. Geophys. Res. Lett. 33, L18316. doi:10.1029/2006GL027120.
Vinnik, L., Farra, V., 2007. Low S velocity atop the 410-km discontinuity and mantle plumes. Earth Planet. Sci. Lett. 262 (3–4), 398–412.
Vinnik, L.P., Kosarev, G.L., Makeyeva, L.I., 1984. Anisotropy in the lithosphere from the observations of SKS and SKKS. Proc. Acad. Sci. USSR 278, 1335–1339.
Vinnik, L.P., Chevrot, S., Montagner, J.-P., Guyot, F., 1999. Teleseismic traveltime residuals in North America and anelasticity of the asthenosphere. Phys. Earth Planet. Inter. 116, 93–103.
Vinnik, L., Reigber, Ch., Aleshin, I.M., Kosarev, G.L., Kaban, M.K., Oreshin, S.I., Roecker, S., 2004. Receiver function tomography of the central Tien Shan. Earth Planet. Sci. Lett. 225, 131–146.
Vinnik, L.P., Foulger, G.R., Du, Z., 2005. Seismic boundaries in the mantle beneath Iceland: a new constraint on temperature. Geophys. J. Int. 160, 533–538. doi:10.1111/j.1365-246X.2005.02529.x.
Vinnik, L., Oreshin, S., Kosarev, G., Kiselev, S., Makeyeva, I., 2009. Mantle anomalies beneath southern Africa: evidence from seismic S and P receiver functions. Geophys. J. Int. 179 (1), 279–298.
Vinnik, L., Ren, Y., Stutzmann, E., Farra, V., Kiselev, S., 2010. Observations of S410p and S350p phases at seismograph stations in California. J. Geophys. Res. 115, B05303. doi:10.1029/2009JB006582.
Wang, Y., Wen, L., Weidner, D., 2008. Upper mantle SH- and P-velocity structures and compositional models beneath southern Africa. Earth Planet. Sci. Lett. 267, 596–608.
Yang, T., Shen, Y., van der Lee, S., Solomon, S.C., Hung, S.-H., 2006. Upper mantle structure beneath the Azores hotspot from finite frequency seismic tomography. Earth Planet. Sci. Lett. 250, 11–26.
Zhu, I., Kanamori, H., 2000. Moho depth variations in southern California from teleseismic receiver functions. J. Geophys. Res. 105 (B2), 2969–2980. doi:10.1029/1999JB900322.